https://doi.org/10.5194/egusphere-2025-192
Preprint. Discussion started: 10 February 2025

Role of precipitation and extreme precipitation events in the surface mass balance variability observed in three ice cores from coastal Dronning Maud Land

Sarah Wauthy[1,2] and Quentin Dalaiden[3,4,5]

[1]Laboratoire de Glaciologie, Département Géosciences, Environnement et Société (DGES), Université libre de Bruxelles (ULB), Brussels, Belgium
[2]Laboratoire G-Time, Département Géosciences, Environnement et Société (DGES), Université Libre de Bruxelles (ULB), Brussels, Belgium
[3]Lemaître Centre for Earth and Climate Research (TECLIM), Earth and Life Institute (ELI), Université catholique de Louvain (UCL), Louvain-la-Neuve, Belgium
[4]Bjerknes Center for Climate Research, Bergen, Norway
[5]Nansen Environmental and Remote Sensing Center (NERSC), Bergen, Norway

Correspondence to: Sarah Wauthy (sarah.wauthy@ulb.be)

Abstract. The Antarctic Ice Sheet (AIS) is the most uncertain contributor to future sea level rise for projections by the end of this century. One of the main drivers of future AIS mass changes is the surface mass balance (SMB) of the ice sheet, which is associated with a number of uncertainties, including its large temporal and spatial variability. The SMB is influenced by a complex interplay of the various processes driving it, including large-scale atmospheric circulation, ice sheet topography, and other interactions between the atmosphere and the snow/ice surface. This spatial and temporal variability is identified in three ice cores located at the crests of adjacent ice rises in coastal Dronning Maud Land, each approximately 90 km apart, which show very contrasting SMB records. In this study, we analyze the role of precipitation and extreme precipitation events (EPEs) in this variability. Our results, based on RACMO2.3 and statistical downscaling techniques, confirm that precipitation is the primary driver of SMB, and that synoptic-scale EPEs play a significant role in controlling interannual variability in precipitation and thus SMB. Shedding light on the intricate nature of SMB variability, our results also demonstrate that precipitation and EPEs alone cannot explain the observed contrasts in SMB records among the three ice core sites and suggest that other processes may be at play. This underscores the importance of adopting comprehensive, interdisciplinary methods, like data assimilation that combines observations and the physics of models, to unravel the underlying mechanisms driving this variability.

1 Introduction

The Antarctic Ice Sheet (AIS) has contributed to about 10 % of the sea level rise observed between 2006 and 2018 and has been losing mass at an accelerating rate until 2016 (Fox-Kemper et al., 2021). Since 2016, the mass loss has not continued to increase due to regional mass gains at the surface, particularly in Dronning Maud Land (Velicogna et al., 2020). A recent study by Wang et al. (2023) reported a total mass gain of 130 Gt yr^{-1} between 2021 and 2022, setting a record for the satellite period. This mass gain, observed over the East AIS and the Antarctic Peninsula, exceeded the basal mass loss in the Amundsen sector of the West AIS, which is driven by the intrusions of warm water masses beneath the ice shelves. According to the Clausius-Clapeyron law, at each degree of warming, a precipitation increase of 7 % should be observed (Krinner et al., 2006; Palerme et al., 2014; Dalaiden et al., 2020). The projected snow accumulation increase in the coming decades might therefore play a pivotal role in mitigating the basal mass loss. Examining surface processes is key to understanding why the ice sheet has gained surface mass in the past years. With an equivalent of 58.0 m of sea level rise (Oppenheimer et al., 2019), the AIS is the largest potential contributor and yet the most uncertain one to the future sea level rise (Kopp et al., 2017). The three main drivers of

https://doi.org/10.5194/egusphere-2025-192
Preprint. Discussion started: 10 February 2025

this future AIS change – sub-shelf melting, ice shelf disintegration, and surface mass balance – are all expected to increase under a warming climate (Fox-Kemper et al., 2021).

Surface mass balance (SMB) in Antarctica is largely dominated by the amount of solid precipitation (van Wessem et al., 2018; Agosta et al., 2019). The effect of higher temperature, referred to as thermodynamics, is one of the three mechanisms controlling precipitation. The two other mechanisms are related to dynamics, which can be further separated into synoptic-scale dynamics and large-scale dynamics (Dalaiden et al., 2020). Synoptic-scale dynamics correspond to short-lived intrusion of maritime air resulting in high precipitation, such as extreme precipitation events (EPEs) which can also be associated with atmospheric rivers (Turner et al., 2019). Atmospheric rivers are defined by the American Meteorological Society as "a long, narrow, and transient corridor of strong horizontal water vapor transport that is typically associated with a low-level jet stream ahead of the cold front of an extratropical cyclone". Large-scale dynamics correspond to the southward moisture transport from lower latitudes due to large-scale atmospheric modes of variability (Marshall et al., 2017).

Unlike thermodynamic changes, dynamical changes induce a strong regional variability due to the interactions of winds with the topography. This for instance explains the high rate of snow accumulation over the eastern part of the Antarctic Peninsula (due to adiabatic cooling; windward side) and the low rate on the leeward side in the western Peninsula (van Wessem et al., 2016). Similarly, ice rises along the Antarctic coastline significantly influence the spatial variability in precipitation, and hence accumulation, over smaller scales, typically spanning a few kilometers (Lenaerts et al., 2014). The orographic uplift on the windward side of the ice rise enhances precipitation, while snow erosion takes place on the leeward side, leading to a local gradient of the SMB distribution across the ice rise (Lenaerts et al., 2014). In the Dronning Maud Land (DML) coastal region, on the Lokeryggen ice rise, a significant contrast between the windward and the leeward sides of an ice rise was observed with a SMB up to 1.5 times higher on the windward side over a 30 year-period (Kausch et al., 2020).

Beyond spatial variability, SMB is also characterized by strong temporal variability. Medley and Thomas (2019) identified an Antarctic-wide snow accumulation increase between 1801 and 2000, which mitigated the 20th century sea level rise by approximately 10 mm. However, these snow accumulation reconstructions strongly vary, both in sign and magnitude, at the regional scale (Medley and Thomas, 2019). While the long-term and large-scale snow accumulation changes are well understood in West Antarctica (e.g., Medley and Thomas, 2019; Dalaiden et al., 2021), the variability in East Antarctica is more complex. Medley and Thomas (2019) found a general increase over the East AIS between 1801 and 2000 but a decrease in the late 20th century, along with strong local trends – some positive, others negative – during the second half of the 20th century. Most of the ice cores in coastal DML show a decreasing SMB trend over recent decades (Kaczmarska et al., 2004; Sinisalo et al., 2013; Schlosser et al., 2014; Altnau et al., 2015; Vega et al., 2016; Ejaz et al., 2021) but an ice core shows a significant increasing trend from mid-20th century (Philippe et al., 2016). A recent study added two new records to the region: one shows a significant decreasing trend, while the other presents a more complex pattern with alternating periods of increases and decreases (Wauthy et al., 2024).

These two new records, along with the one of Philippe et al. (2016), are located at the crests of three adjacent ice rises, each approximately 90 km apart. These records capture significant SMB variability making them ideal locations to study the spatial and temporal variability. The complexity of Antarctic SMB, as well as its historical and contemporary changes, highlight the crucial need for a deeper understanding of the processes involved. Such knowledge is essential for improving our ability to predict the future contribution of Antarctic snow accumulation to global sea-level rise.

https://doi.org/10.5194/egusphere-2025-192
Preprint. Discussion started: 10 February 2025

In this paper, we aim to understand the SMB variability observed at the three ice rises mentioned above and to decipher the processes driving this variability. To achieve this, we use a polar-oriented regional climate model to study the SMB components and their potential trends over the satellite era. We also analyze the role of EPEs in the observed SMBs and their associated synoptic conditions. Finally, we investigate the long-term variability of precipitation using a recent dataset providing an ensemble of simulations at high spatial resolution since 1850.

2 Data and methods

2.1 Ice cores SMB

Three ice cores have been drilled on adjacent ice rises along the Princess Ragnhild coast in DML (see Fig. 1): Derwael ice rise (DIR), Lokeryggen ice rise (LIR), and Hammarryggen ice rise (HIR). The westernmost (HIR) and easternmost (DIR) ice rises are approximately 180 km apart. Note that, from a geomorphological point of view, the Lokeryggen and Hammarryggen ice rises are ice promontories connected to the grounded ice sheet to the south and surrounded by ice shelves to the east, north and west. The IC12 core was drilled in December 2012 at the crest of DIR (−70.24218 °S, 26.34162 °E) and is 120 m long. The FK17 core was drilled during the 2017/2018 austral summer at the crest of LIR (-70.53648° S, 24.07036° E) and is 208 m long. The TIR18 core was drilled during the 2018/2019 austral summer at the crest of HIR (-70.49960° S, 21.88017° E) and is 262 m long. Only the top 120 m of both FK17 and TIR18 cores have been analyzed (Wauthy et al., 2024).

The three ice cores were dated to the end of the eighteenth century at a depth of 120 m (CE 1759 ± 16 years, CE 1793 ± 3 years and 1780 ± 5 years, for IC12, FK17, and TIR18 respectively). Annual layers have been identified using water stable isotopes ($\delta^{18}O$, δD), specific major ions with seasonal signal and electrical conductivity measurement with the identification of volcanic horizons allowing to refine the relative dating. The complete dating procedures are described in Philippe et al. (2016) for IC12 and Wauthy et al. (2024) for FK17 and TIR18. The annual layer thicknesses are obtained from combining raw annual layer thicknesses with density profiles. Subsequently, these thicknesses are corrected for the ice flow deformation effect, which accounts for the horizontal deformation of the ice resulting from the weight of the overlying snow and firn column.

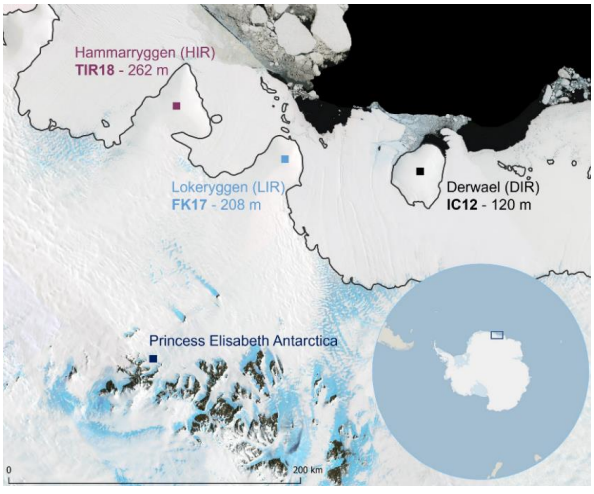

Figure 1: Location of the three ice cores drilled at the crest of the ice rises, from west to east: Hammarryggen (HIR), Lokeryggen (LIR) and Derwael (DIR). Region of the Princess Ragnhild Coast, Dronning Maud Land, East Antarctica. Figure from Wauthy et al. (2024).

https://doi.org/10.5194/egusphere-2025-192
Preprint. Discussion started: 10 February 2025

The mean SMB over 1816–2011 is comparable for IC12, FK17, and TIR18, with respectively 477 mm w.e. yr^{-1}, 532 mm w.e. yr^{-1}, and 504 mm w.e. yr^{-1}. However, the three annual SMB records exhibit pronounced differences regarding the temporal variability (Fig. 2). The IC12 core shows relatively stable SMB from 1750 to 1950, with intermittent interdecadal variability, followed by a significant increase until the end of the record in 2011. In contrast, FK17 presents a more complex pattern with long-term oscillations: an increase from 1793 to about 1825, a decrease until ~1925, another increase and plateau until about 1995, and a recent decreasing trend. TIR18 displays higher variability with no statistically detectable trend before 1850 but exhibits a significant SMB decrease extending to the end of the record in 2018.

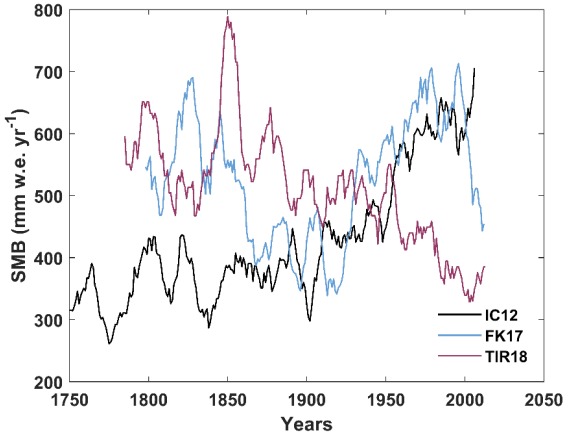

Figure 2: Surface mass balance records from the three ice cores, expressed in millimeter water equivalent per year (IC12 in black, FK17 in blue and TIR18 in burgundy). These have been corrected for vertical strain rates and smoothed using an 11-year running mean. Figure adapted from Wauthy et al. (2024).

2.2 The Regional Atmospheric Climate MOdel (RACMO)

The SMB can be described as in Lenaerts et al. (2019):

$$SMB = P - SU_s - SU_{ds} - ER_{ds} - RU\ , \quad (1)$$

where P corresponds to the total precipitation (snowfall and rain), SU_s represents the surface loss by sublimation and by evaporation, SU_{ds} and ER_{ds} correspond to the sublimation and the erosion/deposition, respectively, of the drifting snow caused by the near-surface winds (i.e., blowing snow), and RU is the meltwater runoff.

We use a regional climate model (RCM) able to accurately simulate surface processes over ice sheets, more specifically the Regional Atmospheric Climate MOdel version 2.3p2 (referred to as RACMO2.3 here) (van Wessem et al., 2018). RACMO2.3 is specifically applied to the polar regions (van Wessem et al., 2018), including a specific regional simulation centered on DML at 5.5 km horizontal resolution (Lenaerts et al., 2014) spanning the 1979–2016 period. This simulation used the ERA-Interim atmospheric reanalysis (Dee et al., 2011) as forcing at its lateral boundaries. To analyze the precipitation component of the SMB at a daily resolution, we use the total precipitation provided by the RACMO2.3 grid cells corresponding to each of the three ice core sites. The grid cells are named following to the ice core sites: IC for IC12 site, FK for FK17 site, and TIR for TIR18 site. A precipitation day is defined as a day with more than 0.02 mm of precipitation (Turner et al., 2019).

2.3 Downscaling

Considering the strong internal variability of the Antarctic climate system (Jones et al., 2016), we make use of a recent statistical downscaling-based dataset extending the time period covered by the RACMO simulation. Such an approach has

https://doi.org/10.5194/egusphere-2025-192
Preprint. Discussion started: 10 February 2025

been performed over the coastal region of DML by Ghilain et al. (2022a) (see for details and specifications). Briefly, this dataset provides daily snowfall by using the high-resolution RACMO simulation and an ensemble of 10 simulations performed with an Earth System Model at low resolution spanning the 1850–2014 period. The 10 downscaled simulations differ by their different initial states, which therefore represent the impact of internal variability of the climate system. We thus base our long-
145 term analysis on this dataset.

3 Results

3.1 SMB components

Major differences are observed between the SMB simulated by RACMO2.3 (black line, Fig. 3) and the ice-core records (grey line, Fig. 3) from 1979 to 2016. RACMO2.3 consistently underestimates SMB compared to ice-core observations, with
150 differences of approximately 200 mm for both FK (36 % of the ice core SMB) and TIR (49 %), and about 265 mm for IC (44 %). Additionally, RACMO2.3 underrepresents interannual variability: its standard deviation ranges from 77 to 103 mm, compared to 135 to 199 mm in the ice-core records. To investigate the drivers of SMB variability, we analyze its components (Eq. 1) using RACMO2.3. Meltwater runoff is negligible, particularly on the grounded ice sheet (van Wessem et al., 2018), so we focus on the four other components: total precipitation (P), surface loss by sublimation (SU_s), sublimation (SU_{ds}) and
155 erosion/deposition caused by drifting snow (ER_{ds}). Figure 3 illustrates the temporal evolution of these components from 1979 to 2016, highlighting their relative contributions to total SMB, for each site.

As expected, precipitation is the main component of the annual mean SMB. For both the IC and FK sites, the erosion by the blowing snow also plays a major role in the mean SMB with a contribution reaching 23.0 % and 34.6 % of the total mean
160 modelled SMB, respectively. In addition, the SMB at the TIR site is governed by the blowing snow-related sublimation (contribution of 19.2 %), which indicates that this site is highly prone to blowing snow. In contrast, the SMB at the FK site is less impacted by the blowing snow, with a smaller contribution to the mean modelled SMB from the erosion (13.2 %) and sublimation (17.1 %).

165 The temporal variability of the SMB is almost entirely controlled by precipitation. The annual SMB variability closely follows year-to-year precipitation at all three sites, with anomalously high/low SMB corresponding to anomalously high/low precipitation (Fig. 3). Precipitation accounts for over 90 % of the SMB variance for each site, with negligible contributions from other components. Thus, according to RACMO2.3, SMB variability is primarily driven by precipitation.

https://doi.org/10.5194/egusphere-2025-192
Preprint. Discussion started: 10 February 2025

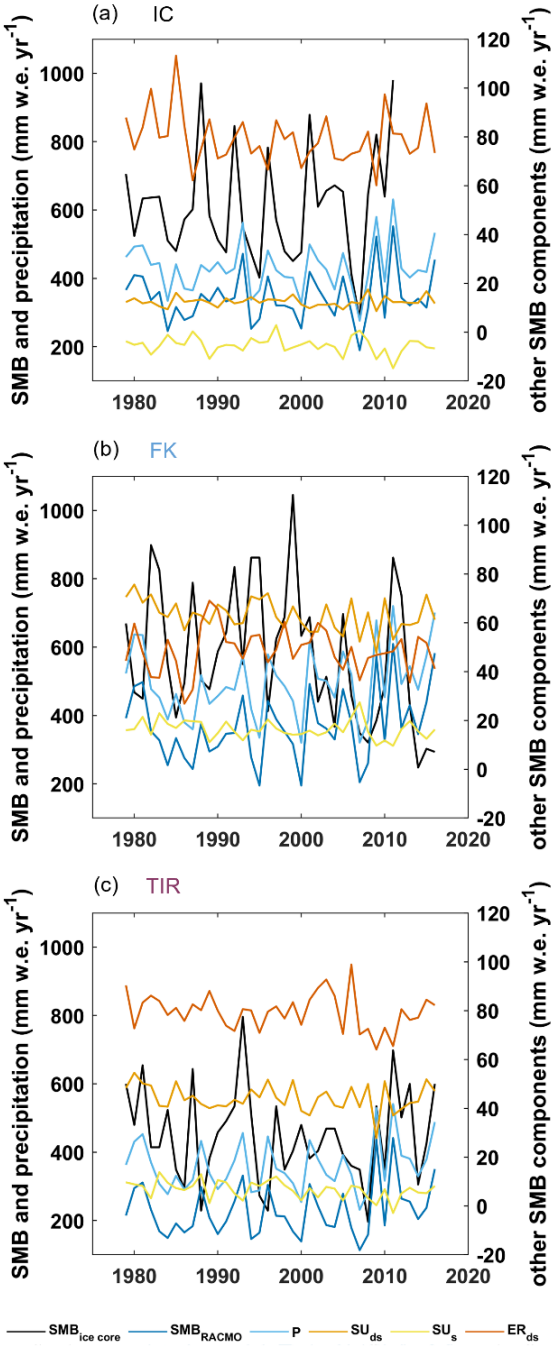

170 **Figure 3: Temporal evolution of the SMB components and SMB derived from the three ice cores between 1979 and 2016 at IC (a), FK (b) and TIR (c), expressed in mm w.e. yr^{-1}. Precipitation and SMBs are represented on the left axis while sublimations and erosion are represented on the right axis.**

https://doi.org/10.5194/egusphere-2025-192
Preprint. Discussion started: 10 February 2025

3.2 Precipitation: spatial variability and temporal trends

Precipitation is the key driver of the SMB variability at our three ice core sites according to RACMO2.3, we thus analyze the annual total precipitation variability over 1979–2016 using RACMO2.3 and the high-resolution precipitation downscaling dataset from Ghilain et al. (2022b, c, d) to study the variability since 1850.

3.2.1 Interannual variability

According to RACMO2.3, snowfall occurs on approximately half of the days during the 1979–2016 period (54 % for FK and TIR, and 62 % for IC). To better understand the spatial distribution of snowfall between sites, the distribution of the precipitation days is examined (Table 1). Specifically, when precipitation occurs at one site, the conditions at the two other sites are evaluated. This approach helps determine whether a snowfall day at one site coincides with dry conditions at another, potentially explaining the opposite signals in the ice-core records. The analysis considers both the number of events and the precipitation quantities: for each site, the proportion of total precipitation occurring during events affecting all three sites, only the specific site, or the site and one other location is calculated.

	Number of events (%)				Quantity (%)			
	all sites	site only	+ site 1	+ site 2	all sites	site only	+ site 1	+ site 2
IC	75.6	13.3	7.7 (FK)	3.4 (TIR)	95.7	1.3	2.5 (FK)	0.5 (TIR)
FK	86.4	1.4	8.9 (IC)	3.3 (TIR)	99.1	0.1	0.6 (IC)	0.2 (TIR)
TIR	87.2	5.5	4.0 (IC)	3.3 (FK)	98.4	0.5	0.3 (IC)	0.8 (FK)

Table 1: Distribution of precipitation days at the three sites using RACMO2.3. An event occurring at one site is categorized differently if it affects all three sites, the considered site only or the considered site and one of the two other sites (in this case, the name in parenthesis indicates which site is the second site impacted). The "number of events" represents the fraction of the total number of events in the category. Quantity represents the percentage of total precipitation that fell at one site based on the event category.

It appears that a significant proportion of precipitation events affects all three sites simultaneously, though IC experiences more events occurring only at this site. However, this characteristic only represents 1.3 % of IC's total precipitation. For all three sites, over 95 % of total precipitation occurs during events affecting the three sites simultaneously. Therefore, RACMO2.3 suggests minimal spatial variability in precipitation across the three sites. This is further supported by the high correlations in annual total precipitation series among the sites (Fig. S1 in the Supplement), with Pearson correlation coefficients greater than 0.85 (0.88 for FK-IC correlation, 0.91 for TIR-IC and 0.93 for TIR-FK).

To examine long-term variability, daily precipitation data from the downscaling dataset have also been analyzed. Overall, the results align with those from RACMO2.3 about the snowfall distribution for the satellite era, confirming the absence of spatial variability in annual precipitation across the three sites, even over longer time scales.

3.2.2 Multi-decadal variability from downscaling

This section examines potential long-term trends and highlights multidecadal variability. Annual snowfall data from 10 ensemble members, along with the ensemble average, are shown for each site in Fig. 4. The results reveal significant multi-decadal variability at all sites but no clear long-term trends, in contrast with ice-core records. The distribution of precipitation anomalies (fluctuations along the mean) at the annual resolution in both outputs of RACMO2.3 and the 10 members from the downscaling is summarized in Table 2. Overall, Table 2 confirms the absence of significant spatial variability in precipitation across the three sites. For both datasets, the three sites show the same anomaly sign (either positive or negative) in over 70 % of cases. FK and TIR are slightly more closely connected, sharing the same anomaly sign more frequently, while IC shows an opposite sign in about 13 % of cases. The remaining cases account for 5–10 %.

https://doi.org/10.5194/egusphere-2025-192
Preprint. Discussion started: 10 February 2025

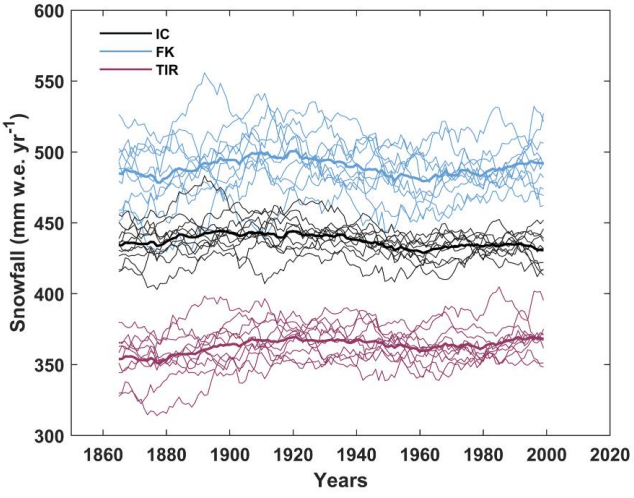

Figure 4: Annual snowfall of the 10 members and average of the 10 members (thick line) at the three sites: IC (in black), FK (in blue) and TIR (in burgundy).

Distribution of precipitation anomalies (%)	+IC +FK +TIR	-IC -FK -TIR	+IC -FK -TIR	-IC +FK -TIR	+IC -FK +TIR	-IC +FK -TIR	-IC +FK +TIR	+IC -FK -TIR
RACMO2.3	31.6	39.5	0	5.3	2.6	7.9	5.3	7.9
Downscaling	32 ± 4	40 ± 4	4 ± 2	4 ± 2	3 ± 2	4 ± 1	6 ± 2	7 ± 2

Table 2: Distribution of precipitation anomalies (% of total cases) at the annual resolution in both outputs of RACMO2.3 and the 10 members average from the downscaling. The "+" sign corresponds to positive anomalies and the "-" sign corresponds to negative anomalies. For the downscaling, the ± standard deviation values represent the variability between the members.

3.3 Extreme Precipitation Events

Besides playing a role in SMB variability, Extreme Precipitation Events (EPEs) have been shown to significantly contribute to the total annual precipitation across Antarctica (Turner et al., 2019). Even though there is not a unique definition of an EPE in the literature (Turner et al., 2019 and references therein), an EPE day is defined here as a day when the total precipitation exceeds a certain percentile value of the total daily precipitation distribution from RACMO2.3 between 1979 and 2016. Here, we use the 95th percentile. Since RACMO2 is able to capture atmospheric rivers (Lenaerts et al., 2014), we use a second percentile (98th) as a proxy for atmospheric rivers that can produce intense localized snowfall when air masses are orographically lifted. Atmospheric rivers rarely occur around Antarctica with an average of 3–3.5 days per year at coastal locations (Wille et al., 2021). EPEs are analyzed to investigate potential spatial and/or temporal trends that might explain the different SMB trends observed in the three ice cores. This analysis is applied to precipitation days from both the RACMO2.3 (1979–2016) and downscaling (1850–2014) datasets.

3.3.1 Contribution of EPEs to the total annual precipitation and to its variability

Annual EPE precipitation is defined as the sum of precipitation during EPEs for each year (mid and dark colors, Fig. 5). For the downscaling dataset, annual EPE snowfall time series are derived for each of the 10 members, and their average is calculated for the three sites. The averages of the 10 members for the 95th percentile and 98th percentile, and the total snowfall are plotted for IC, FK, and TIR in Fig. 5b, 5d, and 5f, respectively.

https://doi.org/10.5194/egusphere-2025-192
Preprint. Discussion started: 10 February 2025

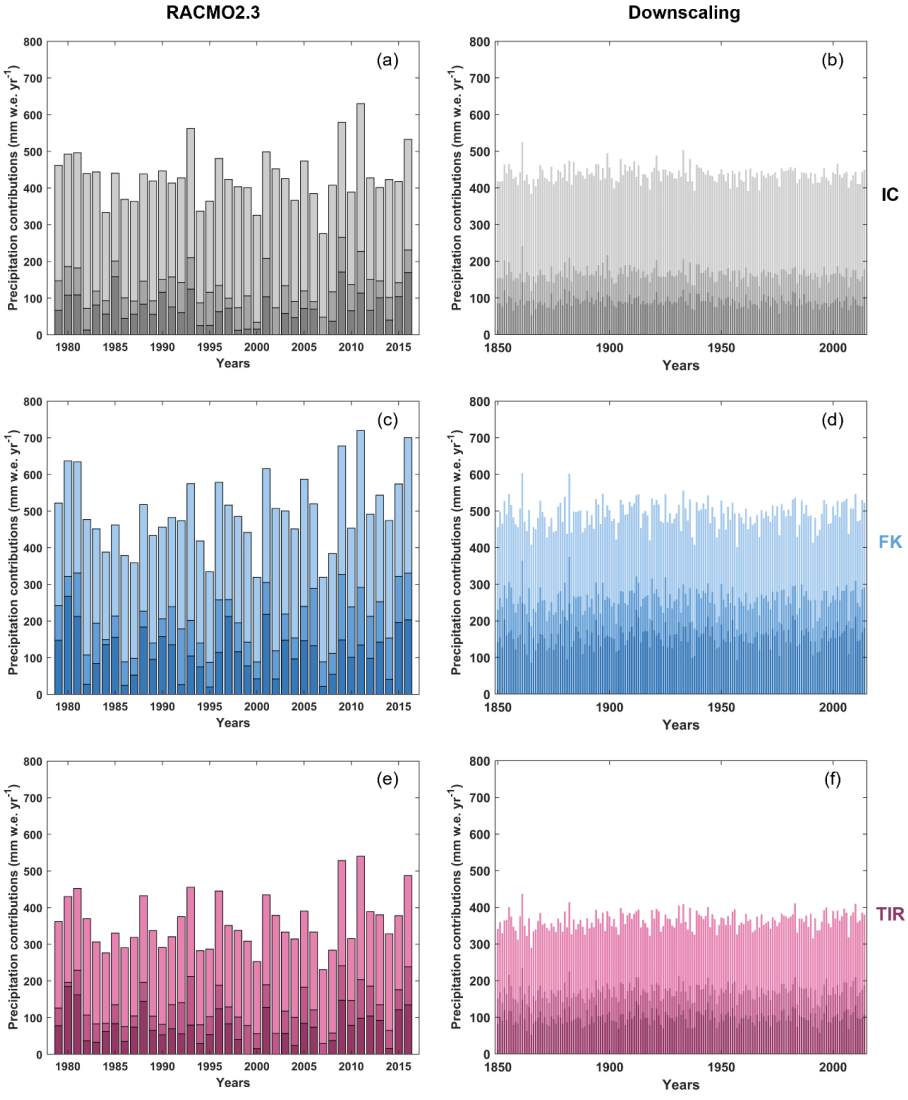

Figure 5: Contributions of the EPEs defined by the 95th and 98th percentiles to the total annual precipitations (RACMO2.3; left panels) and to the total annual snowfalls (downscaling; right panels) at the three sites: IC (a-b), FK (c-d) and TIR (e-f). The contribution of the 98th EPEs is represented by the dark color, the contribution of the 95th EPEs corresponds to the sum of the dark and mid colors (since the 98th EPEs are included in the 95th EPEs), and the total annual precipitation is the sum of the dark, mid, and light colors. Note that for visibility reasons, the standard deviation (representing the variability) between the 10 members of the downscaling dataset is not shown here.

As for the annual precipitation series, correlations are evaluated between the annual EPE precipitation of the three sites. The resulting Pearson correlation coefficients are high for both percentiles, indicating relatively strong correlations between the series. This is especially evident in the RACMO2.3 annual EPE precipitation, with an average coefficient of 0.79 for the 95th percentile (0.74 for FK-IC correlation, 0.82 for TIR-IC and 0.82 for TIR-FK). Albeit the correlation still remains high when considering the 98th percentile, we notify a weaker relationship (0.69 for FK-IC, 0.75 for TIR-IC and 0.80 for TIR-FK). The correlation coefficients are lower in the downscaling dataset (average r=0.57 for the 95th percentile and 0.68 for the 98th percentile). All these coefficients are consistently lower than those of the annual precipitation series, this suggests that EPE impacts are more localized compared to the average conditions. Similar to the total annual precipitation series, the annual EPE precipitation series from RACMO2.3 show no significant temporal trend at any site for both percentiles. A similar conclusion

https://doi.org/10.5194/egusphere-2025-192
Preprint. Discussion started: 10 February 2025

can be drawn from the downscaling dataset, although one to two ensemble members are characterized by significant trends (not shown), no general pattern has been identified. The number of EPE days also shows no significant temporal trends either (not shown).

The contributions of EPEs to the total annual precipitation vary in space and time (Table 3) in both RACMO2.3 (Fig. 5a, 5c, and 5e) and downscaling datasets (Fig. 5b, 5d, and 5f).

Average contribution (%)	95th percentile			98th percentile		
	IC	FK	TIR	IC	FK	TIR
RACMO2.3	30.0	40.0	35.2	15.6	22.4	19.1
Downscaling	37 ± 8	51 ± 9	46 ± 9	20 ± 7	30 ± 11	26 ± 10
Variance (%)						
RACMO2.3	50.8	57.5	54.2	35.4	38.9	36.3
Downscaling	68 ± 5	83 ± 5	78 ± 5	42 ± 6	60 ± 6	53 ± 7

Table 3: Average contribution (upper rows) and variance (lower rows) of EPEs to the total annual precipitations (RACMO2.3) or snowfalls (downscaling) for the three sites, expressed in %. For the downscaling, the ± standard deviation values represent the variability between the members.

Table 3 illustrates that EPEs consistently contribute more to the total annual precipitation at FK than at the other sites. The EPE variance accounts for more than one-third to more than two-thirds of the SMB variance. This confirms the critical role of EPEs in the SMB variability. However, no significant temporal trends are observed in the EPEs contributions to the total annual precipitations, at all sites, for the two EPEs thresholds, and in both RACMO2.3 and downscaling datasets. Consequently, this rules out EPEs as the cause of the different SMB trends observed in the three ice cores.

3.3.2 Synoptic patterns during EPEs

Figure 6 presents the mean daily sea-level pressure anomalies (relative to the 1979–2022 monthly climatology) for all 95th percentile EPEs at the three sites, retrieved from the ERA5 atmospheric reanalysis. The synoptic conditions reveal a large negative sea-level pressure anomaly centered over Dronning Maud Land, with an associated high sea-level pressure located in the East of Droning Maud Land. This dipole structure forms a blocking ridge over the region east of the ice rises and brings a large quantity of moisture from the lower latitudes to the ice core sites. This is a typical synoptic pattern during EPEs (Turner et al., 2019; Wille et al., 2021; Simon et al., 2024). The large-scale synoptic pattern shows no significant differences across the three sites. Similar observations are made for EPEs defined with the 98th percentile (see Fig. S2 in the Supplement). According to RACMO2.3 along with ERA5, the synoptic conditions associated with the EPEs therefore cannot explain the spatial variability observed from ice-core records.

https://doi.org/10.5194/egusphere-2025-192
Preprint. Discussion started: 10 February 2025

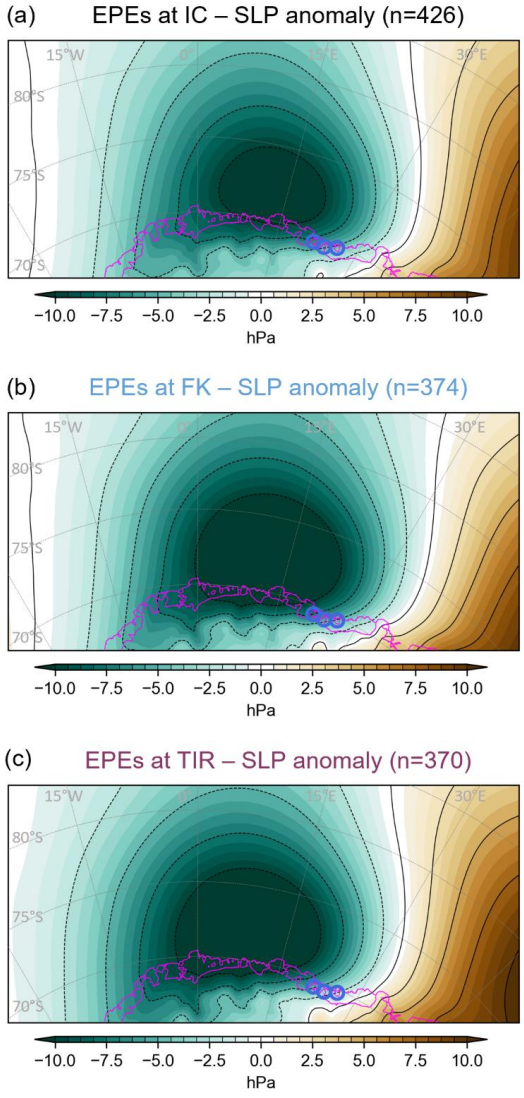

Figure 6: Maps of the mean daily sea-level pressure anomaly (SLP) for all 95th percentile EPEs at the three sites: (a) IC, (b) FK, and (c) TIR. The number in parentheses corresponds to the number of EPE days. Blue colors indicate negative anomaly (i.e., low pressure) and brown colors indicate positive anomaly (i.e., high pressure). The anomalies are relative to monthly climatology calculated over the 1979–2022 period. The location of the three ice cores is shown as circles.

3.4 Frequency distributions of precipitation anomalies

A particularly high precipitation event at one site might result in abnormally low precipitation at the two other sites, possibly explaining the different SMB trends observed in the three ice cores. Similarly to the well-documented foehn effect over the Antarctic Peninsula, it is reasonable to hypothesize that a large precipitation event at one site could result in reduced precipitation at other locations. This phenomenon arises from the interaction between topography and wind. As the primary moisture in the air is released over the first site (in form of snow), the remaining air holds less humidity, leading to drier conditions and reduced precipitation at downstream sites (along the wind flow). To explore this, we study the frequency distributions of precipitation anomalies at the two other sites on dates corresponding to EPEs at the first site. Precipitation

https://doi.org/10.5194/egusphere-2025-192
Preprint. Discussion started: 10 February 2025

anomalies are calculated for each site by subtracting the average value of precipitation days from each daily precipitation value. Results are shown here for the 95th percentile EPEs, and in Sect. S3 in the Supplement for the 98th percentile EPEs.

3.4.1 Evaluation of the frequency distributions

The frequency distributions of precipitation anomalies are presented in Fig. 7, with RACMO2.3 results on the left panels and downscaling results on the right. When an EPE occurs at one site, the two other sites may receive either below-average precipitation (negative anomalies), more precipitation than their EPE threshold, or an average amount of precipitation. The first two scenarios are of particular interest to test the hypothesis of a drier air mass reaching the other sites after precipitating at the first site. Table 4 summarizes the results for both datasets. In this table, "EPEs" refers to the percentage of cases where the other sites receive more precipitation than their site-specific EPE threshold and "Neg. anom." refers to the percentage of cases with below-average precipitation.

RACMO2.3 (%)	EPEs at IC		EPEs at FK		EPEs at TIR	
	FK	TIR	IC	TIR	IC	FK
EPEs	58.0	58.9	66.0	70.9	68.1	71.9
Neg. anom.	6.6	9.2	0.5	0	1.1	1.1
Downscaling (%)	EPEs at IC		EPEs at FK		EPEs at TIR	
	FK	TIR	IC	TIR	IC	FK
EPEs	58 ± 4	57 ± 3	59 ± 4	66 ± 6	59 ± 3	66 ± 6
Neg. anom.	4 ± 2	5 ± 2	3 ± 1	1 ± 1	4 ± 1	3 ± 3

Table 4: Distribution of the precipitation anomalies at two sites when there is a 95th percentile EPE at the third site, in %, for both the RACMO2.3 and downscaling datasets. For the downscaling, the average of the 10 members is shown, as well as the standard deviation to highlight the variability between members. See text for more explanations on the "EPEs" and "Neg. anom." (i.e., negative anomalies) categories.

For the RACMO2.3 results, EPEs at the IC site (Fig. 7a and Table 4) coincide less frequently to EPEs at the two other sites and more often result in negative precipitation anomalies (an average of 34 events) compared to the EPEs at FK and TIR (2–4 events on average). This therefore suggests that an EPE at IC may lead to drier conditions at the FK and TIR sites, possibly due to a reduced moisture availability in the air mass following intense precipitation at the IC site. Similar observations are made from the 98th percentile EPEs (Sect. S3 in the Supplement).

For the EPEs at FK and TIR sites (Fig. 7c and 7e), the distribution of the events as well as their frequency are very close (Table 4). In particular, the shape of the distribution shapes of the corresponding events at IC are very similar (black line in Fig. 7c and 7e). This indicates that precipitation variability at the FK and TIR sites evolves in the same direction according to RACMO2.3. However, the distribution shapes for corresponding events at TIR/FK when EPEs occur at FK/TIR significantly differ, with a longer distribution tail for FK, indicating larger precipitation anomalies. This is also evident from the frequency distributions of EPEs occurring at IC (Fig. 7a), where FK and TIR have similar percentages of events above their respective EPEs thresholds but the distribution tail (e.g., beyond 20 mm) is higher at FK. Overall, this indicates that FK is more subject to large precipitation anomalies than the other sites, a finding confirmed by the downscaling results (Fig. 7b and 7f).

https://doi.org/10.5194/egusphere-2025-192
Preprint. Discussion started: 10 February 2025

315 Overall, the majority of the EPEs at one site coincide with EPEs at the two other sites, indicating that precipitation events generally affect all sites. This rules out the hypothesis of a drier air mass reaching the other sites after precipitating at the first site, at least according to RACMO2.3. All these observations further support the previous hypothesis that neither precipitations nor EPEs explain the contrasting SMB trends in the three ice cores and instead point to the influence of global atmospheric pathways.

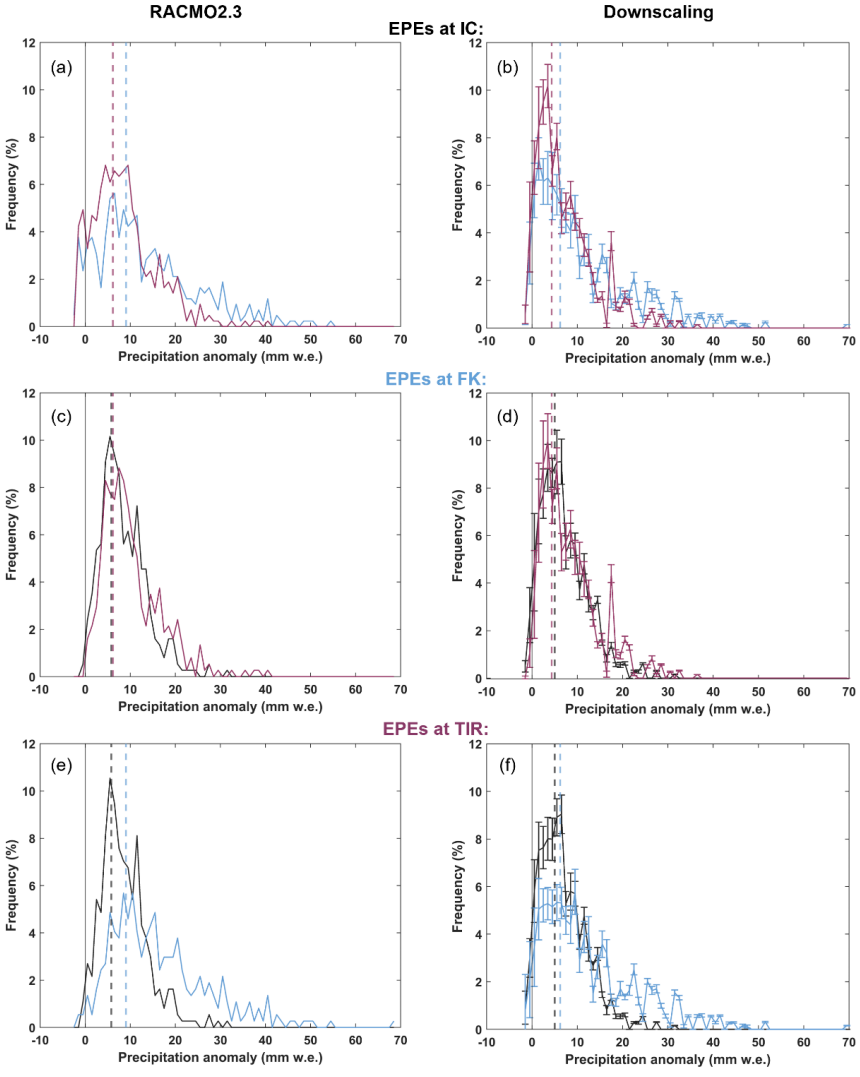

320 **Figure 7: Frequency distributions of precipitation anomalies (calculated as the precipitation – the average value of precipitation series) at the two other sites corresponding to the dates of 95th percentile EPEs at (a-b) IC, (c-d) FK and (e-f) TIR, using the RACMO2.3 data series (left panels) and the downscaling data series (right panels). Colors of the distribution correspond to each ice core, with IC in black, FK in blue, and TIR in burgundy. The vertical dashed lines represent the EPE thresholds corrected for**
325 **anomalies (EPE threshold – the average value of precipitation series).**

3.4.2 Synoptic patterns during EPEs at IC and negative anomalies at FK and TIR

Although global atmospheric pathways are predominantly observed, the 95th percentile EPEs at IC are more likely to result in negative precipitation anomalies at the FK and TIR sites. Specifically, there are 28 and 39 cases of negative anomalies at FK and TIR, respectively, compared to no case to only 4 negative anomaly events when EPEs occur at FK or TIR. Few of these
330 cases happen with the 98th percentile EPEs (see Table S1 in the Supplement) and are therefore not discussed further. Figure 8

https://doi.org/10.5194/egusphere-2025-192
Preprint. Discussion started: 10 February 2025

thus focuses on the synoptic patterns associated with 95th percentile EPEs at IC that led to negative anomalies at the FK and TIR sites. These events appear to correspond to occasional, very localized situations where air masses precipitate at the IC site and arrive drier at FK and TIR sites. This contrasts with the strong and deep low-pressure system shown in Fig. 6a, which represents the atmospheric conditions during all EPEs at IC. The pressure gradient is considerably weaker in Fig. 8, indicating reduced wind strength and less effective moisture transport to FK and TIR.

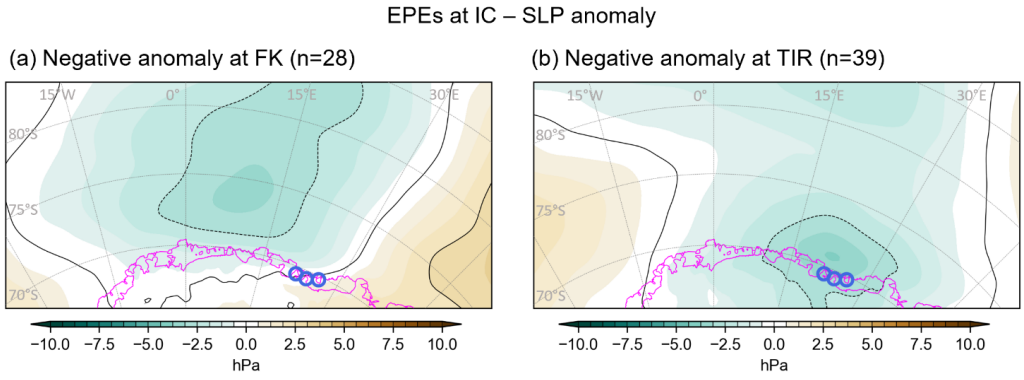

Figure 8: Maps of the sea level pressure anomaly (SLP) during 95th percentile EPEs at the IC site leading to negative precipitation anomalies at (a) FK and (b) TIR. The number in parentheses corresponds to the number of cases. Blue colors indicate negative pressure anomaly, and brown colors indicate positive anomaly.

4 Discussion

East Antarctica has recently emerged as the source of most uncertainties regarding Antarctica's potential to mitigate sea level rise (Eswaran et al., 2024). In the coastal DML region, ice-core records exhibit contrasting SMB trends. Multiple ice cores show a decreasing SMB trend over recent decades (Kaczmarska et al., 2004; Sinisalo et al., 2013; Schlosser et al., 2014; Altnau et al., 2015; Vega et al., 2016; Medley and Thomas, 2019; Ejaz et al., 2021), while one ice core indicates a significant increasing trend since the half of the 20th century (Philippe et al., 2016). Regional reconstruction by Thomas et al. (2017) suggests a significant positive SMB trend from 1800 to 2000. Recent observations by Wauthy et al. (2024) show one ice core with oscillating SMB and another with a marked decline. The three ice cores analyzed in this study, those of Philippe et al. (2016) and Wauthy et al. (2024), indeed exhibit highly contrasting SMB records, underscoring the strong regional and temporal variability of the SMB and its intricate nature. This complexity is, in part, attributable to the multitude of processes involved. As previously emphasized, a better understanding of the SMB is crucial to improve the projections of Antarctica's future contribution, and potential mitigation, to sea level rise.

Both RACMO2.3 and long-term downscaled simulations indicate no spatial variability or temporal trends in precipitation across our three study sites, highlighting a significant model-data discrepancy with the SMB records from the ice cores. The frequency distributions of precipitation anomalies and the analysis of atmospheric conditions during EPEs suggest a common atmospheric pathway of air masses resulting in similar precipitation patterns at all three sites. This finding excludes the hypothesis of decreasing precipitation intensity along the air mass trajectory. Overall, the different temporal trends observed in the three SMB ice-core records cannot be attributed to precipitation-related processes based on these models.

Furthermore, this study focuses on the importance of spatial variability by comparing the SMB records at the three ice-core sites. Multiple studies emphasize the determining role of orography in shaping the EPEs occurrence and the precipitation distribution during these events (Turner et al., 2019; Gehring et al., 2022; Simon et al., 2024). The importance of finer scale surface topography is also underscored in the general precipitation pattern. For instance, Dattler et al. (2019) highlighted

https://doi.org/10.5194/egusphere-2025-192
Preprint. Discussion started: 10 February 2025

substantial spatial variability at the local, sub-grid, scale (< 25 km) related to wind-driven snow redistribution. This type of relationship between accumulation variability and surface topography could enable downscaling reanalysis accumulation product to 1 km grid in the future. Noël et al. (2023) presented a statistically downscaled version of RACMO2.3 SMB at 2 km resolution and compared it with the original 27 km resolution (1979-2021). While this downscaling relatively enhances the SMB at the continental scale (3 %) and reconciles modelled and satellite mass change, some significant differences between the two SMB products persist at the local scale. For example, the 2 km SMB product is approximately 300 mm w.e. yr^{-1} higher than the 27 km product at the IC site. This is the order of the difference observed between the 5.5 km RACMO2.3 product and the IC12-derived SMB record (~265 mm w.e. yr^{-1}). This is consistent with the findings of Mottram et al. (2021), who reported underestimation of SMB in the low-elevation coastal regions of Antarctica by the 27 km RACMO product.

The SMB outputs were compared for the three sites using both the 5.5 km and 2 km resolutions and expressed in terms of relative differences (in %) in Fig. S4 in the Supplement. The average difference between the 5.5 km-SMB and the 2 km-SMB was found to be -315 mm w.e. yr^{-1}, +80 mm w.e. yr^{-1}, and -49 mm w.e. yr^{-1} for IC, FK, and TIR, respectively. The interannual variability remains largely consistent between the two products, with changes of +3.3 %, -5.5 %, and +4.4 %, for IC, FK, and TIR respectively. Most importantly, the correlations between the three SMB time series remain strong in the 2 km product, with Pearson correlation coefficients of 0.87 for IC-FK, 0.86 for IC-TIR, and 0.96 for FK-TIR, comparable to those derived from the 5.5 km output. This confirms a more pronounced connection between the SMBs at FK and TIR. These results, in conjunction with the use of the 5.5 km RACMO2.3 product for generating the statistically downscaled snowfall timeseries employed here, provide evidence of the suitability of the 5.5 km products in this study.

The underestimation of the SMB by models is also evident when comparing the ice core-derived SMBs with those obtained from RACMO2.3 at 5.5 km resolution (Fig. 3). All three ice core sites are situated in local minimum SMB relative to their surrounding ice rise environments (Kausch et al., 2020; Cavitte et al., 2022). Consequently, the discrepancy between RACMO outputs and ice core observations would increase further if the ice core SMBs were adjusted to reflect the consistently lower SMB at the drilling site compared to the mean SMB value of the entire ice rise, estimated to be 70-150 mm w.e. yr^{-1} higher (Cavitte et al., 2022). Although local dynamic conditions at these drilling sites may influence the absolute accumulation values, the temporal variability is well represented by ice-core records (Cavitte et al., 2022). However, this temporal variability appears to be underestimated in model outputs in comparison to the ice core observations, highlighting a limitation in the model representation of SMB interannual variability.

One hypothesis to explain the spatial model-data discrepancy could be related to the missing small-scale processes, such as the underestimation of the blowing snow impacts on SMB in RACMO (Agosta et al., 2019). In a recent study, Gadde and van de Berg (2024) updated the blowing snow module in RACMO2.3 and reevaluated its contribution to the modeled SMB at a 27 km resolution. Their findings indicate that the contribution of blowing snow sublimation increased by 52 % for the integrated AIS during the period 2000-2012 in the updated version of RACMO2.3 compared to the previous version. Concomitantly, a reduction of 1.2 % is observed in the integrated AIS SMB. Moreover, significant changes in blowing snow transport and total sublimation are observed in some coastal regions, including in the vicinity of our study sites. This suggests that the blowing snow term was underestimated in the RACMO2.3 version used in this study, yet also that there are high uncertainties associated with this term. The implementation of such small-scale processes and the specific, local scale, topography of the ice rises in models is a challenging task. Wind speed can be particularly high at some ice rises (e.g., annual mean wind speed of 8–10 m s^{-1} in the FK area; Simon et al., 2024), likely leading to strong erosion and snow transport. Misrepresenting the effect of blowing snow could partly explain the different trends in the three ice-core records.

https://doi.org/10.5194/egusphere-2025-192
Preprint. Discussion started: 10 February 2025

In summary, the contrasting SMB records from the three ice cores cannot be attributed to differences in precipitation or EPEs patterns, according to state-of-the-art regional climate models. Furthermore, it can be concluded that a common regional atmospheric circulation pattern similarly influences all three sites. However, results of precipitation anomaly distributions indicate that, rarely, certain EPEs at the IC site occasionally lead to negative precipitation anomalies – indicative of drier conditions – at the FK and TIR sites.

It is important to note that both ice core observations and model outputs are subject to uncertainties and limitations. The ice core SMB records, for instance, are only representative of a limited area, approximately 200 to 500 meters in radius around the drilling site, and consistently exhibit lower SMB values than the mean across the entire ice rise. For models, RACMO2.3 (on which the downscaling method is based) misses local, sub-grid, scale processes, even at a resolution of 5.5 km. This limitation likely contributes to the lower spatial and temporal variability observed in model outputs. Finally, the downscaling dataset of Ghilain et al. (2022a) may also substantially underestimate circulation changes due to its reliance on RACMO2.3 outputs, which are based on the satellite period) and exhibit a strong correlation between sites. This raises the possibility that past circulation changes, which could account for the trends observed in the ice cores, are not accurately captured. The statistical downscaling indeed assumes a stationary relationship between precipitation and circulation, which may not be valid over longer timescales.

Consequently, processes other than precipitation are probably driving these SMB contrasts. These could include multi-decadal variability, which may be underestimated in the dataset of Ghilain et al. (2022a), local-scale processes such as blowing snow and erosion-deposition dynamics, or processes not included in atmospheric models, such as surface ice dynamics. Future research could focus on these processes, for example through the use of data assimilation methods that combine observational data (typically SMB from the ice cores) with the physics of climate models. This approach would allow for an evaluation of the ability of this method to reproduce the SMB variability observed in the ice-core records.

5 Conclusions

The AIS is a potential significant contributor to future global sea level rise, making it crucial to understand the mechanisms governing its SMB for accurate projections of future sea level changes. Our investigation into the SMB variability observed at three ice rises in coastal East Antarctica reveals complex interactions between atmospheric processes and local-scale dynamics. The analysis, based on a combination of regional climate modelling and statistical downscaling techniques, sheds light on the intricate nature of SMB variability. While previous studies have emphasized the importance of precipitation, including its spatial and temporal distribution, our findings suggest that precipitation alone cannot fully account for the observed contrasts in SMB records among the three ice core sites.

Our findings indicate that synoptic-scale EPEs play a significant role in controlling interannual variability in precipitation and SMB. These events contribute substantially to the total annual precipitation, particularly in coastal regions, underscoring their importance in shaping SMB patterns. However, the absence of significant temporal trends in precipitation and EPEs across our study sites suggests that other processes may be driving the observed SMB contrasts.

Local-scale processes, such as blowing snow and erosion-deposition dynamics, may contribute to SMB spatial variability, as suggested by the discrepancies between ice core observations and model outputs. Additionally, the influence of surface ice dynamics, not fully captured by current models, cannot be discounted. Future research efforts should focus on integrating observational data, such as SMB records from ice cores, with advanced modelling techniques, including data assimilation methods. This approach has the potential to improve our understanding of SMB dynamics and refining projections of Antarctic ice mass change and its implications for global sea level rise.

https://doi.org/10.5194/egusphere-2025-192
Preprint. Discussion started: 10 February 2025

Our study underscores the complexity of Antarctic SMB variability and highlights the necessity for comprehensive, interdisciplinary approaches to elucidate the underlying processes driving these variations. Only through continued research can we enhance our ability to accurately predict the future evolution of the Antarctic Ice Sheet and its contribution to sea level rise.

Data availability

The SMB and precipitation datasets from RACMO2.3 at a 5.5 km resolution are available from Willem Jan van de Berg upon request. The high-resolution precipitation downscaling from Ghilain et al. (2022a), are available on Zenodo under Creative Commons Attribution 4.0 International Public License. The daily fields are separated into three parts: https://doi.org/10.5281/ZENODO.6355455 for Part 1, https://doi.org/10.5281/ZENODO.6359385 for Part 2, and https://doi.org/10.5281/ZENODO.6362299 for Part 3. Sea-level pressure fields from ERA5 can be retrieved at Copernicus Climate Change Service (C3S) Climate Data Store (https://cds.climate.copernicus.eu/datasets/reanalysis-era5-single-levels?tab=overview).

Author contribution

SW and QD designed the study. QD provided most of the raw data and made the SLP anomalies maps. SW performed the analysis and made the other figures. SW and QD both discussed the results and contributed equally to the writing of the manuscript.

Competing interests

The authors declare that they have no conflict of interest.

Acknowledgements

The authors would like to thank Hugues Goosse and Jean-Louis for their insightful guidance and their critical reading of the manuscript, as well as Willem Jan van de Berg for sharing the RACMO2.3 outputs and Nicolas Ghilain for providing valuable advice on handling the downscaling data.

Financial support

During the course of the study, QD was a Research Fellow within the F.R.S.-F.N.R.S. (Belgium) and SW was supported by the Mass2Ant project (Belgian Science Policy Office - BELSPO, contract no. BR/165/A2/Mass2Ant) and the PARAMOUR project (under the Excellence of Science (EOS) program supported by the F.N.R.S. and the F.W.O. (Belgium); grant no. O0100718F, EOS ID no. 30454083).

References

Agosta, C., Amory, C., Kittel, C., Orsi, A., Favier, V., Gallée, H., Van Den Broeke, M. R., Lenaerts, J. T. M., Van Wessem, J. M., van de Berg, W. J., and Fettweis, X.: Estimation of the Antarctic surface mass balance using the regional climate model MAR (1979–2015) and identification of dominant processes, The Cryosphere, 13, 281–296, https://doi.org/10.5194/tc-13-281-2019, 2019.

Altnau, S., Schlosser, E., Isaksson, E., and Divine, D.: Climatic signals from 76 shallow firn cores in Dronning Maud Land, East Antarctica, The Cryosphere, 9, 925–944, https://doi.org/10.5194/tc-9-925-2015, 2015.

Cavitte, M. G. P., Goosse, H., Wauthy, S., Kausch, T., Tison, J.-L., Van Liefferinge, B., Pattyn, F., Lenaerts, J. T. M., and Claeys, P.: From ice core to ground-penetrating radar: representativeness of SMB at three ice rises along the Princess Ragnhild Coast, East Antarctica, J. Glaciol., 68, 1221–1233, https://doi.org/10.1017/jog.2022.39, 2022.

Dalaiden, Q., Goosse, H., Lenaerts, J. T. M., Cavitte, M. G. P., and Henderson, N.: Future Antarctic snow accumulation trend is dominated by atmospheric synoptic-scale events, Commun Earth Environ, 1, 62, https://doi.org/10.1038/s43247-020-00062-x, 2020.

Dalaiden, Q., Goosse, H., Rezsöhazy, J., and Thomas, E. R.: Reconstructing atmospheric circulation and sea-ice extent in the West Antarctic over the past 200 years using data assimilation, Clim Dyn, 57, 3479–3503, https://doi.org/10.1007/s00382-021-05879-6, 2021.

Dattler, M. E., Lenaerts, J. T. M., and Medley, B.: Significant Spatial Variability in Radar-Derived West Antarctic Accumulation Linked to Surface Winds and Topography, Geophysical Research Letters, 46, 13126–13134, https://doi.org/10.1029/2019GL085363, 2019.

Dee, D. P., Uppala, S. M., Simmons, A. J., Berrisford, P., Poli, P., Kobayashi, S., Andrae, U., Balmaseda, M. A., Balsamo, G., Bauer, P., Bechtold, P., Beljaars, A. C. M., Van De Berg, L., Bidlot, J., Bormann, N., Delsol, C., Dragani, R., Fuentes, M., Geer, A. J., Haimberger, L., Healy, S. B., Hersbach, H., Hólm, E. V., Isaksen, L., Kållberg, P., Köhler, M., Matricardi, M., McNally, A. P., Monge-Sanz, B. M., Morcrette, J. -J., Park, B. -K., Peubey, C., De Rosnay, P., Tavolato, C., Thépaut, J. -N., and Vitart, F.: The ERA-Interim reanalysis: configuration and performance of the data assimilation system, Quart J Royal Meteoro Soc, 137, 553–597, https://doi.org/10.1002/qj.828, 2011.

Ejaz, T., Rahaman, W., Laluraj, C. M., Mahalinganathan, K., and Thamban, M.: Sea Ice Variability and Trends in the Western Indian Ocean Sector of Antarctica During the Past Two Centuries and Its Response to Climatic Modes, JGR Atmospheres, 126, e2020JD033943, https://doi.org/10.1029/2020JD033943, 2021.

Eswaran, A., Truax, O. J., and Fudge, T. J.: 20th-Century Antarctic Sea Level Mitigation Driven by Uncertain East Antarctic Accumulation History, Geophysical Research Letters, 51, e2023GL106991, https://doi.org/10.1029/2023GL106991, 2024.

Fox-Kemper, B., Hewitt, H. T., Xiao, C., Aðalgeirsdóttir, G., Drijfhout, S. S., Edwards, T. L., Golledge, N. R., Hemer, M., Kopp, R. E., Krinner, G., Mix, A., Notz, D., Nowicki, S., Nurhati, I. S., Ruiz, L., Sallée, J.-B., Slangen, A. B. A., and Yu, Y.: Ocean, Cryosphere and Sea Level Change, in: Climate Change 2021 – The Physical Science Basis: Working Group I Contribution to the Sixth Assessment Report of the Intergovernmental Panel on Climate Change, Cambridge University Press, Cambridge, United Kingdom and New York, NY, USA, 1211–1362, https://doi.org/10.1017/9781009157896.011, 2021.

Gadde, S. and van de Berg, W. J.: Contribution of blowing-snow sublimation to the surface mass balance of Antarctica, The Cryosphere, 18, 4933–4953, https://doi.org/10.5194/tc-18-4933-2024, 2024.

Gehring, J., Vignon, É., Billault-Roux, A., Ferrone, A., Protat, A., Alexander, S. P., and Berne, A.: Orographic Flow Influence on Precipitation During an Atmospheric River Event at Davis, Antarctica, JGR Atmospheres, 127, e2021JD035210, https://doi.org/10.1029/2021JD035210, 2022.

Ghilain, N., Vannitsem, S., Dalaiden, Q., Goosse, H., De Cruz, L., and Wei, W.: Large ensemble of downscaled historical daily snowfall from an earth system model to 5.5 km resolution over Dronning Maud Land, Antarctica, Earth Syst. Sci. Data, 14, 1901–1916, https://doi.org/10.5194/essd-14-1901-2022, 2022a.

Ghilain, N., Vannitsem, S., Dalaiden, Q., Goosse, H., and De Cruz, L.: MASS2ANT Snowfall Dataset (Downscaling @5.5km over Dronning Maud Land, Antarctica, 1850 - 2014): Daily fields (Part 1), https://doi.org/10.5281/ZENODO.6355455, 2022b.

Ghilain, N., Vannitsem, S., Dalaiden, Q., Goosse, H., and De Cruz, L.: MASS2ANT Snowfall Dataset (Downscaling @5.5km over Dronning Maud Land, Antarctica, 1850 - 2014): Daily fields (Part 2), https://doi.org/10.5281/ZENODO.6359385, 2022c.

https://doi.org/10.5194/egusphere-2025-192
Preprint. Discussion started: 10 February 2025

Ghilain, N., Vannitsem, S., Dalaiden, Q., Goosse, H., and De Cruz, L.: MASS2ANT Snowfall Dataset (Downscaling @5.5km over Dronning Maud Land, Antarctica, 1850 - 2014): Daily fields (Part 3), https://doi.org/10.5281/ZENODO.6362299, 2022d.

Jones, J. M., Gille, S. T., Goosse, H., Abram, N. J., Canziani, P. O., Charman, D. J., Clem, K. R., Crosta, X., De Lavergne, C., Eisenman, I., England, M. H., Fogt, R. L., Frankcombe, L. M., Marshall, G. J., Masson-Delmotte, V., Morrison, A. K., Orsi, A. J., Raphael, M. N., Renwick, J. A., Schneider, D. P., Simpkins, G. R., Steig, E. J., Stenni, B., Swingedouw, D., and Vance, T. R.: Assessing recent trends in high-latitude Southern Hemisphere surface climate, Nature Clim Change, 6, 917–926, https://doi.org/10.1038/nclimate3103, 2016.

Kaczmarska, M., Isaksson, E., Karlöf, L., Winther, J.-G., Kohler, J., Godtliebsen, F., Olsen, L. R., Hofstede, C. M., Van Den Broeke, M. R., Van De Wal, R. S. W., and Gundestrup, N.: Accumulation variability derived from an ice core from coastal Dronning Maud Land, Antarctica, Ann. Glaciol., 39, 339–345, https://doi.org/10.3189/172756404781814186, 2004.

Kausch, T., Lhermitte, S., Lenaerts, J. T. M., Wever, N., Inoue, M., Pattyn, F., Sun, S., Wauthy, S., Tison, J.-L., and van de Berg, W. J.: Impact of coastal East Antarctic ice rises on surface mass balance: insights from observations and modeling, The Cryosphere, 14, 3367–3380, https://doi.org/10.5194/tc-14-3367-2020, 2020.

Kopp, R. E., DeConto, R. M., Bader, D. A., Hay, C. C., Horton, R. M., Kulp, S., Oppenheimer, M., Pollard, D., and Strauss, B. H.: Evolving Understanding of Antarctic Ice-Sheet Physics and Ambiguity in Probabilistic Sea-Level Projections, Earth's Future, 5, 1217–1233, https://doi.org/10.1002/2017EF000663, 2017.

Krinner, G., Magand, O., Simmonds, I., Genthon, C., and Dufresne, J.-L.: Simulated Antarctic precipitation and surface mass balance at the end of the twentieth and twenty-first centuries, Clim Dyn, 28, 215–230, https://doi.org/10.1007/s00382-006-0177-x, 2006.

Lenaerts, J. T. M., Brown, J., Van Den Broeke, M. R., Matsuoka, K., Drews, R., Callens, D., Philippe, M., Gorodetskaya, I. V., Van Meijgaard, E., Reijmer, C. H., Pattyn, F., and Van Lipzig, N. P. M.: High variability of climate and surface mass balance induced by Antarctic ice rises, J. Glaciol., 60, 1101–1110, https://doi.org/10.3189/2014JoG14J040, 2014.

Lenaerts, J. T. M., Medley, B., Van Den Broeke, M. R., and Wouters, B.: Observing and Modeling Ice Sheet Surface Mass Balance, Reviews of Geophysics, 57, 376–420, https://doi.org/10.1029/2018RG000622, 2019.

Marshall, G. J., Thompson, D. W. J., and Van Den Broeke, M. R.: The Signature of Southern Hemisphere Atmospheric Circulation Patterns in Antarctic Precipitation, Geophysical Research Letters, 44, https://doi.org/10.1002/2017GL075998, 2017.

Medley, B. and Thomas, E. R.: Increased snowfall over the Antarctic Ice Sheet mitigated twentieth-century sea-level rise, Nature Clim Change, 9, 34–39, https://doi.org/10.1038/s41558-018-0356-x, 2019.

Mottram, R., Hansen, N., Kittel, C., Van Wessem, J. M., Agosta, C., Amory, C., Boberg, F., van de Berg, W. J., Fettweis, X., Gossart, A., Van Lipzig, N. P. M., Van Meijgaard, E., Orr, A., Phillips, T., Webster, S., Simonsen, S. B., and Souverijns, N.: What is the surface mass balance of Antarctica? An intercomparison of regional climate model estimates, The Cryosphere, 15, 3751–3784, https://doi.org/10.5194/tc-15-3751-2021, 2021.

Noël, B., Van Wessem, J. M., Wouters, B., Trusel, L., Lhermitte, S., and Van Den Broeke, M. R.: Higher Antarctic ice sheet accumulation and surface melt rates revealed at 2 km resolution, Nat Commun, 14, 7949, https://doi.org/10.1038/s41467-023-43584-6, 2023.

Oppenheimer, M., Glavovic, B. C., Hinkel, J., Van De Wal, R. S. W., Magnan, A. K., Abd-Elawad, A., Cai, R., Cifuentes-Jara, M., DeConto, R., Ghosh, T., Hay, J., Isla, F., Marzeion, B., Meyssignac, B., and Sebesvari, Z.: Sea Level Rise and Implications for Low-Lying Islands, Coasts and Communities, in: The Ocean and Cryosphere in a Changing Climate: Special Report of the Intergovernmental Panel on Climate Change, Cambridge University Press, https://doi.org/10.1017/9781009157964, 2019.

Palerme, C., Kay, J. E., Genthon, C., L'Ecuyer, T., Wood, N. B., and Claud, C.: How much snow falls on the Antarctic ice sheet?, The Cryosphere, 8, 1577–1587, https://doi.org/10.5194/tc-8-1577-2014, 2014.

https://doi.org/10.5194/egusphere-2025-192
Preprint. Discussion started: 10 February 2025

Philippe, M., Tison, J.-L., Fjøsne, K., Hubbard, B., Kjær, H. A., Lenaerts, J. T. M., Drews, R., Sheldon, S. G., De Bondt, K., Claeys, P., and Pattyn, F.: Ice core evidence for a 20th century increase in surface mass balance in coastal Dronning Maud Land, East Antarctica, The Cryosphere, 10, 2501–2516, https://doi.org/10.5194/tc-10-2501-2016, 2016.

Schlosser, E., Anschütz, H., Divine, D., Martma, T., Sinisalo, A., Altnau, S., and Isaksson, E.: Recent climate tendencies on an East Antarctic ice shelf inferred from a shallow firn core network, JGR Atmospheres, 119, 6549–6562, https://doi.org/10.1002/2013JD020818, 2014.

Simon, S., Turner, J., Thamban, M., Wille, J. D., and Deb, P.: Spatiotemporal Variability of Extreme Precipitation Events and Associated Atmospheric Processes Over Dronning Maud Land, East Antarctica, JGR Atmospheres, 129, e2023JD038993, https://doi.org/10.1029/2023JD038993, 2024.

Sinisalo, A., Anschütz, H., Aasen, A. T., Langley, K., Von Deschwanden, A., Kohler, J., Matsuoka, K., Hamran, S. E., Øyan, M., Schlosser, E., Hagen, J. O., Nøst, O. A., and Isaksson, E.: Surface mass balance on Fimbul ice shelf, East Antarctica: Comparison of field measurements and large-scale studies, JGR Atmospheres, 118, https://doi.org/10.1002/jgrd.50875, 2013.

Thomas, E. R., Van Wessem, J. M., Roberts, J., Isaksson, E., Schlosser, E., Fudge, T. J., Vallelonga, P., Medley, B., Lenaerts, J., Bertler, N., Van Den Broeke, M. R., Dixon, D. A., Frezzotti, M., Stenni, B., Curran, M., and Ekaykin, A. A.: Regional Antarctic snow accumulation over the past 1000 years, Clim. Past, 13, 1491–1513, https://doi.org/10.5194/cp-13-1491-2017, 2017.

Turner, J., Phillips, T., Thamban, M., Rahaman, W., Marshall, G. J., Wille, J. D., Favier, V., Winton, V. H. L., Thomas, E., Wang, Z., Van Den Broeke, M., Hosking, J. S., and Lachlan-Cope, T.: The Dominant Role of Extreme Precipitation Events in Antarctic Snowfall Variability, Geophysical Research Letters, 46, 3502–3511, https://doi.org/10.1029/2018GL081517, 2019.

van Wessem, J. M., Ligtenberg, S. R. M., Reijmer, C. H., van de Berg, W. J., van den Broeke, M. R., Barrand, N. E., Thomas, E. R., Turner, J., Wuite, J., Scambos, T. A., and Van Meijgaard, E.: The modelled surface mass balance of the Antarctic Peninsula at 5.5 km horizontal resolution, The Cryosphere, 10, 271–285, https://doi.org/10.5194/tc-10-271-2016, 2016.

van Wessem, J. M., van de Berg, W. J., Noël, B. P. Y., Van Meijgaard, E., Amory, C., Birnbaum, G., Jakobs, C. L., Krüger, K., Lenaerts, J. T. M., Lhermitte, S., Ligtenberg, S. R. M., Medley, B., Reijmer, C. H., Van Tricht, K., Trusel, L. D., Van Ulft, L. H., Wouters, B., Wuite, J., and Van Den Broeke, M. R.: Modelling the climate and surface mass balance of polar ice sheets using RACMO2 – Part 2: Antarctica (1979–2016), The Cryosphere, 12, 1479–1498, https://doi.org/10.5194/tc-12-1479-2018, 2018.

Vega, C. P., Schlosser, E., Divine, D. V., Kohler, J., Martma, T., Eichler, A., Schwikowski, M., and Isaksson, E.: Surface mass balance and water stable isotopes derived from firn cores on three ice rises, Fimbul Ice Shelf, Antarctica, The Cryosphere, 10, 2763–2777, https://doi.org/10.5194/tc-10-2763-2016, 2016.

Velicogna, I., Mohajerani, Y., A, G., Landerer, F., Mouginot, J., Noel, B., Rignot, E., Sutterley, T., Van Den Broeke, M., van Wessem, M., and Wiese, D.: Continuity of Ice Sheet Mass Loss in Greenland and Antarctica From the GRACE and GRACE Follow-On Missions, Geophysical Research Letters, 47, e2020GL087291, https://doi.org/10.1029/2020GL087291, 2020.

Wang, W., Shen, Y., Chen, Q., and Wang, F.: Unprecedented mass gain over the Antarctic ice sheet between 2021 and 2022 caused by large precipitation anomalies, Environ. Res. Lett., 18, 124012, https://doi.org/10.1088/1748-9326/ad0863, 2023.

Wauthy, S., Tison, J.-L., Inoue, M., El Amri, S., Sun, S., Fripiat, F., Claeys, P., and Pattyn, F.: Spatial and temporal variability of environmental proxies from the top 120 m of two ice cores in Dronning Maud Land (East Antarctica), Earth Syst. Sci. Data, 16, 35–58, https://doi.org/10.5194/essd-16-35-2024, 2024.

Wille, J. D., Favier, V., Gorodetskaya, I. V., Agosta, C., Kittel, C., Beeman, J. C., Jourdain, N. C., Lenaerts, J. T. M., and Codron, F.: Antarctic Atmospheric River Climatology and Precipitation Impacts, JGR Atmospheres, 126, e2020JD033788, https://doi.org/10.1029/2020JD033788, 2021.